*Proceedings of the*
*Annual Stability Conference*
*Structural Stability Research Council*
*Atlanta, Georgia, April 21-24, 2020*

# A continuation on the influence of loaded width on web compression buckling

Jacob Witte[1], Kadir Sener[2], Amit Varma[3]

**Abstract**
This paper presents a continuation and conclusion to an experimental and numerical study on the web compression buckling strength of steel wide-flange members subjected to concentric loads spread over a length wider than member depths. The previous study focused on conducting experimental tests at a fixed load-width to investigate the behavior and response while undergoing web compression buckling. The previous experimental study tested specimens with variable lengths to develop benchmark numerical models to obtain insight into behavior and use in parametric study. The benchmarked numerical models accounted for imperfections and residual stresses to accurately estimate the web compression buckling strength of the specimens. This paper focuses on developing analytical buckling equations based on the results obtained from the numerical parametric study investigations on the compression buckling strength of wide flange members. The parameters considered in the studies were the load width, web height, web thickness, and the angle of the applied load. Findings from the experimental and numerical studies provided data necessary to propose new set of equations to the existing AISC specification equations for local web compression buckling to include the effect of load width.

## 1. Introduction

This paper explores the effect of loading width on the web compression buckling strength of unstiffened wide-flange (I-shaped sections) members subjected to uniform load. This loading condition commonly occurs for orthogonally intersecting through members where compression members are bearing on both flanges. In cases where field conditions make welding bearing stiffeners difficult, the web compression buckling strength of that through member becomes very important for transferring the forces to the adjacent member. However, the current AISC 360-16 design equation was developed for use in beam-to-column moment connections where the loaded width is very small compared to the depth of the section. When the loaded width is large relative to the section depth, AISC 360 provides an alternative calculation approach in the Commentary to evaluate the girder web as a column in accordance with Chapter E. This paper aims to evaluate, then improve upon, these recommendations by providing a different analysis procedure rooted in the classical theoretical studies conducted on the ultimate compressive strength of rectangular plates under uniform load.

[1] Project Engineer, Lynch, Harrison, & Brumleve, Inc., <jwitte@lhb-eng.com>
[2] Assistant Professor, Auburn University, <sener@auburn.edu>
[3] Karl H. Kettlelhut Professor in Civil Engineering, Purdue University, <ahvarma@purdue.edu>

## 2. Project Background and Previous Research

This paper is a continuation of the experimental and computational research conducted by Sener et al. (2019). Sener et al. (2019) featured the experimental testing of web compression buckling over load widths greater than the section depth. The experimental results were later used for developing benchmarked numerical models. In this paper, these benchmarked models are used to conduct numerical parametric studies. This study will build upon the observed experimental behavior and response, and focus on the numerical parametric study results. An analytical approach to calculate the web compression buckling strength is also developed, where the methodology and results are presented and summarized throughout the remainder of this paper. The most recent research conducted on this topic by Menkulasi & Farzana (2019) were referred in this study for comparisons. Their study also performed a similar numerical analysis of web compression buckling and the results are to supplement the findings in this study.

## 3. Numerical Parametric Study

### *3.1 Objectives and Scope*

The objective of this study was to generate additional data through numerical analyses to be used towards developing an analytical calculation procedure. The investigated parameters were the (i) section depth and thickness of the web, (ii) load width, and (iii) angle of applied load. The variation in section dimensions (depth and width) was accounted for by investigating 4 commonly used wide-flange beam sections of different web slenderness ($h/t_w$) ratios: W18x40, W18x60, W16x26, and W24x84. Each beam section was subjected to load widths as a function of their section depth, $d$, ranging from $0.5d$ to $2.5d$ by increments of $0.5d$. 3 angles of load application, $\theta$, were also investigated: 0, 30, and 45 degrees measured from the vertical axis (i.e. plane perpendicular to the specimen length). These parameters are summarized in the following table.

Table 1: Summary of Parameters

| Parameters | Values | | | | |
|---|---|---|---|---|---|
| Section | W18x60 | W24x84 | W18x40 | W16x26 | |
| $h/t_w$ | 38.7 | 45.9 | 50.9 | 56.8 | |
| $w$ | $0.5d$ | $1.0d$ | $1.5d$ | $2.0d$ | $2.5d$ |
| $\theta$ | 0 | 30 | 45 | | |

### *3.2 Modeling and Analysis Procedure*

The numerical model consisted solely of the wide-flange section specimen subjected to the applied load. Rigid plates were used as the boundary elements to apply and resist the load to the specimen. The load was applied to the rigid plate adjacent the top flange surface at the desired load length and transferred to the specimen through contact. The rigid plate at the opposite flange was held in place by a fixed boundary condition. The top and bottom rigid plates were also restrained against rotation, twisting and translation in the other directions. In summary, translations and rotations other than the vertical movement of the top flange was restrained by boundary conditions imposed on the rigid plates. The specimens had a total length of 10 times the loaded width, $w$, to minimize the effects of end conditions.

The analyses were performed using Abaqus and its implicit solution method in a sequential procedure. First, a linear perturbation buckling analysis was performed to obtain the critical elastic

buckling load and the critical buckling modes via an eigenvalue analysis. The buckling mode shapes obtained from the eigenvalue analysis were used in the following stress analysis as the imposed initial imperfections. As a conservative approach, initial imperfection was based only on the first eigenmode shape and the magnitude was determined based on the physical measurements performed on the specimens during the experimental phase. The stress analysis was performed using the Riks method while accounting for the nonlinear material and geometric imperfections to obtain the final buckling strength.

*3.3 Benchmarked Modeling Details*

This section describes the details of the modeling methodology used for developing benchmarked models according to the experimental tests performed by the authors (Witte 2019). In the benchmarking stage, the specimens and loading were modeled to mimic the experiments. The specimens were modeled to the appropriate lengths and the rigid plate was extended to the entire top flange of the specimen, since the specimens were loaded uniformly. The material properties used in the benchmarking models were defined according to the parameters described in the previous study (Sener et al. 2019). Sensitivity studies were also performed to evaluate the adequacy of the selected element size for the benchmarking analysis.

The specimens were modeled using C3D20R solid elements, which is a 20 node, quadratic, reduced integration solid element. This element was chosen for its ability to accurately capture the stress and deformations during the buckling of members. Having quadratic shape function for the element permits the use of a coarse mesh density without sacrificing accuracy in the analysis, thus increasing the computational efficiency. Additionally, this element type is rarely susceptible to hour-glassing, making the element suitable for flexural-buckling analyses.

The benchmarking analyses were conducted by varying the peak imperfection for a range of amplitudes that varied from 5%-30% of the web thickness (0.05-0.3*$t_w$). This range corresponds to 0.01575 to 0.0945 inches of imperfection for a W18x40 member. Residual stresses had minimal influence in the analysis results, because their direction of influence is primarily along the longitudinal axis of the beam and the loading was applied in the transverse direction.

The load versus out-of-plane (OOP) web displacement plots generated in the analysis are compared with the experimental results in Figure 1. The comparisons indicate almost identical response in terms of both stiffness and final strength. The magnitude of applied imperfection that yielded the most accurate result varied for each of the specimen. The load versus displacement curves for a 1-inch and 2-inch mesh size were identical in all 3 plots, thus the 2-inch mesh size was used at a much lower computational cost.

*3.4 Parametric Model Creation*

Numerical parametric study was established through python scripting for both steps in the sequential Riks analysis procedure that resulted in a total of 120 analyses. The same steel material property was used throughout the analysis with the yield strength and ultimate strength set equal to 55 and 75 ksi respectively. The effects of strain hardening and variation in the yield plateau were not investigated because of their minimal effect and rare use in other design applications (Menkulasi & Farzana 2019). Initial imperfection was not considered as a parameter in the investigations due to its wide variability and difficulty in measurement. Instead, all analyses

incorporated imperfection levels equal to $0.13t_w$ as the average of the imperfection measured for the specimens tested in the experimental phase.

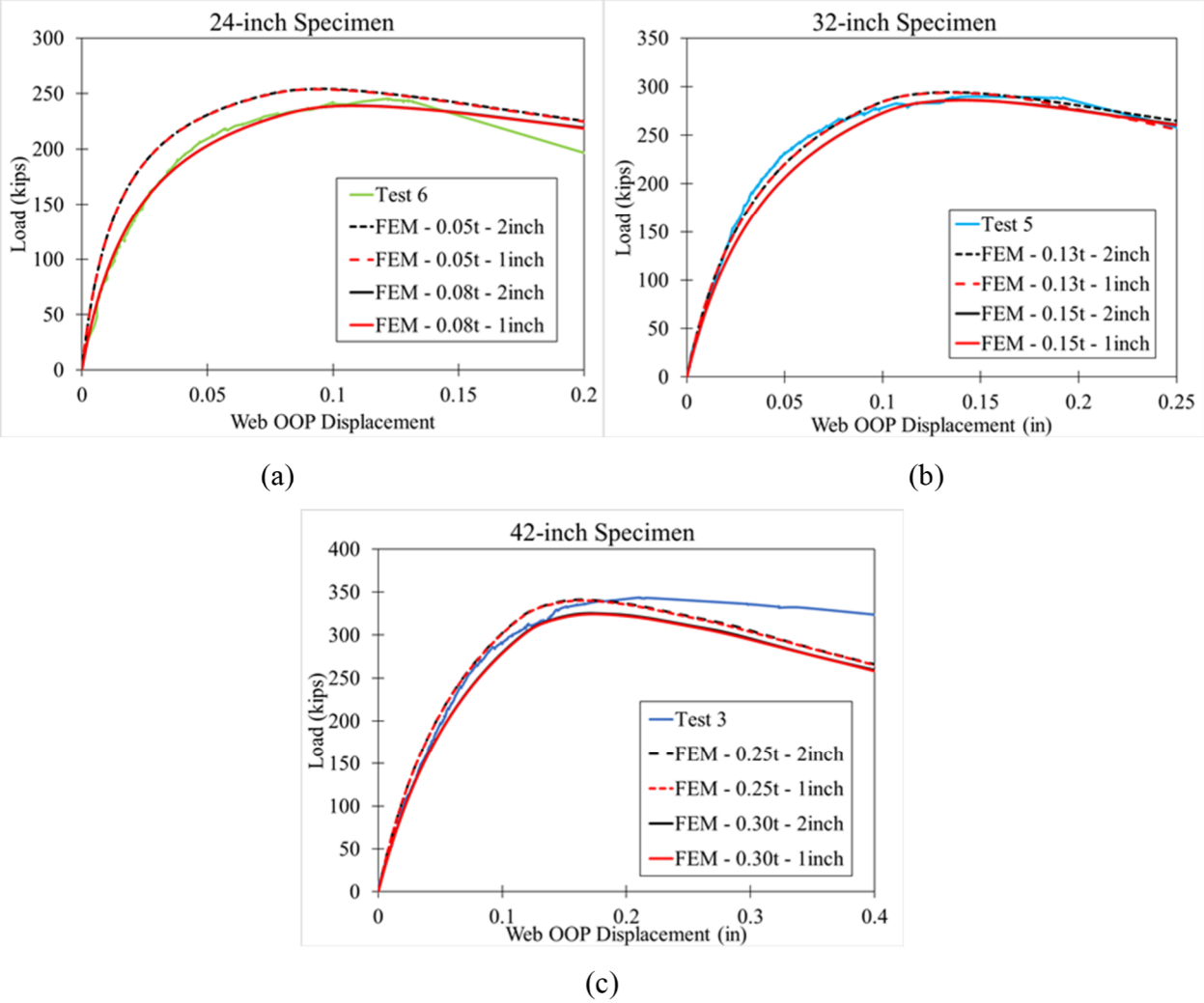


Figure 1: Comparison of Parametric Study Benchmarking Results to Experimental Results from (a) Test 6, (b) Test 5, and (c) Test 3 from Witte (2019)

## 4. Results of Parametric Study

The analysis results returned the critical elastic buckling load and ultimate buckling strength for the investigated cases. All results are compiled in Table 2 and organized by beam size, load width, and angle of applied load. As expected, increasing the loaded width $w$ results in higher total buckling loads. Increasing the angle of application also tends to increase the ultimate buckling strength. Additionally, the heavier specimens had the greatest difference between the elastic buckling capacity and ultimate load from the analysis, suggesting that inelastic buckling was more prevalent on the governing failure mode of these specimens.

Table 2: Numerical Parametric Study Results

| Analysis | Section | *w/d* | *w* | θ | Ultimate Strength | Elastic Buckling Load |
|---|---|---|---|---|---|---|
| # | Name | | in | deg | kips | kips |
| 1 | W24x84 | 0.5 | 12.05 | 0 | 441.1 | 694.2 |
| 2 | W24x84 | 1.0 | 24.10 | 0 | 573.8 | 869.9 |
| 3 | W24x84 | 1.5 | 36.15 | 0 | 758.3 | 1104.2 |
| 4 | W24x84 | 2.0 | 48.20 | 0 | 957.5 | 1362.9 |
| 5 | W24x84 | 2.5 | 60.25 | 0 | 1162.5 | 1634.1 |
| 6 | W24x84 | 0.5 | 12.05 | 30 | 482.3 | 852.1 |
| 7 | W24x84 | 1.0 | 24.10 | 30 | 597.0 | 1037.3 |
| 8 | W24x84 | 1.5 | 36.15 | 30 | 787.6 | 1300.1 |
| 9 | W24x84 | 2.0 | 48.20 | 30 | 1004.9 | 1598.7 |
| 10 | W24x84 | 2.5 | 60.25 | 30 | 1230.3 | 1915.4 |
| 11 | W24x84 | 0.5 | 12.05 | 45 | 572.1 | 1074.6 |
| 12 | W24x84 | 1.0 | 24.10 | 45 | 603.8 | 1231.1 |
| 13 | W24x84 | 1.5 | 36.15 | 45 | 779.1 | 1517.3 |
| 14 | W24x84 | 2.0 | 48.20 | 45 | 1003.6 | 1876.4 |
| 15 | W24x84 | 2.5 | 60.25 | 45 | 1243.3 | 2271.3 |
| 16 | W18x60 | 0.5 | 9.10 | 0 | 322.7 | 610.7 |
| 17 | W18x60 | 1.0 | 18.20 | 0 | 422.1 | 763.6 |
| 18 | W18x60 | 1.5 | 27.30 | 0 | 559.3 | 968.0 |
| 19 | W18x60 | 2.0 | 36.40 | 0 | 708.7 | 1193.6 |
| 20 | W18x60 | 2.5 | 45.50 | 0 | 862.3 | 1430.2 |
| 21 | W18x60 | 0.5 | 9.10 | 30 | 344.1 | 750.5 |
| 22 | W18x60 | 1.0 | 18.20 | 30 | 426.0 | 909.6 |
| 23 | W18x60 | 1.5 | 27.30 | 30 | 562.7 | 1137.9 |
| 24 | W18x60 | 2.0 | 36.40 | 30 | 719.2 | 1397.8 |
| 25 | W18x60 | 2.5 | 45.50 | 30 | 881.4 | 1673.9 |
| 26 | W18x60 | 0.5 | 9.10 | 45 | 405.5 | 950.2 |
| 27 | W18x60 | 1.0 | 18.20 | 45 | 423.2 | 1082.6 |
| 28 | W18x60 | 1.5 | 27.30 | 45 | 549.0 | 1327.8 |
| 29 | W18x60 | 2.0 | 36.40 | 45 | 705.8 | 1638.1 |
| 30 | W18x60 | 2.5 | 45.50 | 45 | 871.5 | 1981.2 |

Table 2: Numerical Parametric Study Results - Continued

| Analysis | Section | *w/d* | *w* | *θ* | Ultimate Strength | Elastic Buckling Load |
|---|---|---|---|---|---|---|
| # | Name | | in | deg | kips | kips |
| 31 | W18x40 | 0.5 | 8.95 | 0 | 195.9 | 267.5 |
| 32 | W18x40 | 1.0 | 17.90 | 0 | 252.6 | 334.6 |
| 33 | W18x40 | 1.5 | 26.85 | 0 | 331.7 | 424.1 |
| 34 | W18x40 | 2.0 | 35.80 | 0 | 417.3 | 522.9 |
| 35 | W18x40 | 2.5 | 44.75 | 0 | 504.9 | 626.7 |
| 36 | W18x40 | 0.5 | 8.95 | 30 | 220.0 | 326.4 |
| 37 | W18x40 | 1.0 | 17.90 | 30 | 270.1 | 398.1 |
| 38 | W18x40 | 1.5 | 26.85 | 30 | 352.8 | 498.8 |
| 39 | W18x40 | 2.0 | 35.80 | 30 | 448.7 | 612.9 |
| 40 | W18x40 | 2.5 | 44.75 | 30 | 548.9 | 734.1 |
| 41 | W18x40 | 0.5 | 8.95 | 45 | 262.2 | 407.7 |
| 42 | W18x40 | 1.0 | 17.90 | 45 | 282.5 | 470.7 |
| 43 | W18x40 | 1.5 | 26.85 | 45 | 359.2 | 581.2 |
| 44 | W18x40 | 2.0 | 35.80 | 45 | 459.8 | 718.6 |
| 45 | W18x40 | 2.5 | 44.75 | 45 | 570.9 | 869.5 |
| 46 | W16x26 | 0.5 | 7.85 | 0 | 122.5 | 144.0 |
| 47 | W16x26 | 1.0 | 15.70 | 0 | 156.1 | 187.2 |
| 48 | W16x26 | 1.5 | 23.55 | 0 | 204.2 | 237.4 |
| 49 | W16x26 | 2.0 | 31.40 | 0 | 255.6 | 292.9 |
| 50 | W16x26 | 2.5 | 39.25 | 0 | 308.2 | 351.2 |
| 51 | W16x26 | 0.5 | 7.85 | 30 | 139.6 | 178.7 |
| 52 | W16x26 | 1.0 | 15.70 | 30 | 169.6 | 221.3 |
| 53 | W16x26 | 1.5 | 23.55 | 30 | 220.8 | 278.8 |
| 54 | W16x26 | 2.0 | 31.40 | 30 | 279.7 | 343.2 |
| 55 | W16x26 | 2.5 | 39.25 | 30 | 340.9 | 411.5 |
| 56 | W16x26 | 0.5 | 7.85 | 45 | 167.3 | 217.3 |
| 57 | W16x26 | 1.0 | 15.70 | 45 | 184.7 | 257.9 |
| 58 | W16x26 | 1.5 | 23.55 | 45 | 230.7 | 232.4 |
| 59 | W16x26 | 2.0 | 31.40 | 45 | 295.0 | 402.3 |
| 60 | W16x26 | 2.5 | 39.25 | 45 | 365.9 | 487.8 |

## 5. Analytical (Closed-form) Analysis Procedure

The analysis procedure was developed using the numerical parametric study results presented in Section 4 of this paper as well as the results from a similar parametric study conducted by Menkulasi & Farzana (2019). The data points from both sources are differentiated on all relevant figures and tables.

### *5.1 Evaluation of Current AISC Recommendations*

The current AISC 360-16 web compression buckling equation can be found in Chapter J.10 as Equation J10-8 and is shown below.

$$R_n = \frac{24 * t_w^3 \sqrt{E * f_y}}{h} * Q_f \quad (1)$$

The AISC commentary also suggests, in lieu of this equation, the web should be designed as a compression member according to Chapter E when the loaded width is not small compared to the depth of the section. For the purposes of this comparison, any loaded width that was greater than or equal to half of the section depth was considered "not small." When considering the boundary conditions of the equivalent column, the flanges were assumed to create a fixed-fixed condition. The analyses results obtained from the parametric study and other researchers are compared with the calculation based on design of compression members of the specification is presented in the 1-to-1 plot below in Figure 2.

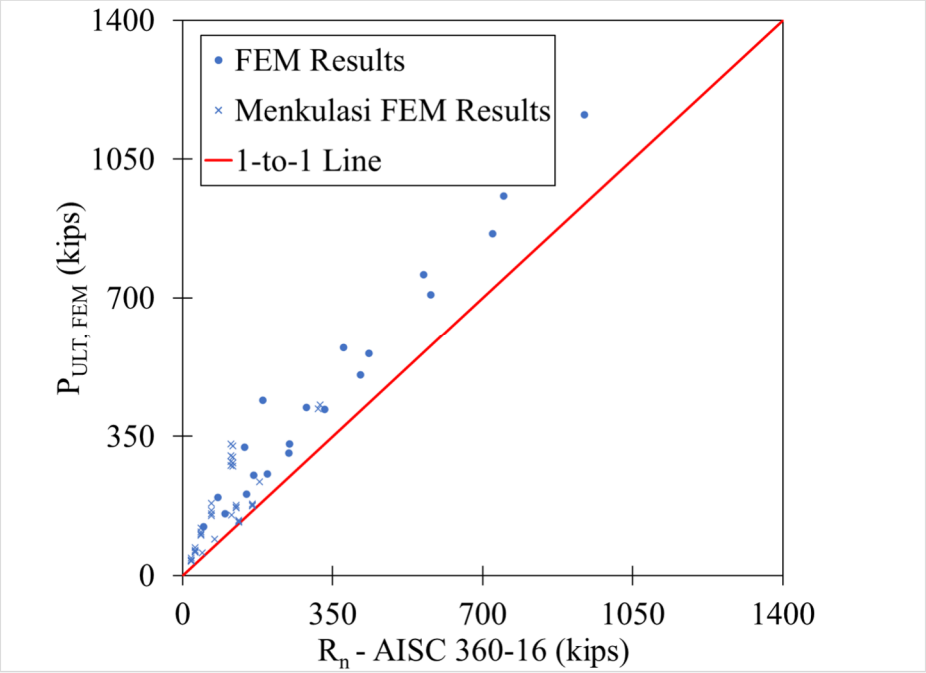


Figure 2: 1-to-1 Comparison Plot of the Numerical Data to Existing AISC Provisions

Figure 2 indicates that almost all of the numerical data points lie above the 1-to-1 line, meaning that the code specification conservatively estimates the strength of most of the analyzed cases. The AISC approach of calculating the web compression buckling strength based on the column member provisions (Chapter E) predicts conservative estimations. It is also noted that, the

predicted strengths yield more accurate strength estimations for smaller loaded widths than for larger loaded widths.

*5.2 Redefining the Problem*

Classical solutions were combined with semiempirical methods to develop a closed-form prediction analytical method for web compression buckling. The webs subjected to load can be treated as a rectangular plate with dimensions $a$, $b$, and $t_w$. The ultimate compressive force capacity of the web can then be calculated using similar methods as for rectangular plates. These methods involve calculating a critical elastic buckling load, a slenderness parameter, and a relationship between plastic yielding, inelastic buckling, and elastic buckling as a function of the slenderness parameter.

The height of the web plate, $a$, is the unstiffened height of the web, $h$, defined as the clear distance between the flanges minus the fillet or corner radius. The width of the effective plate, $b$, is defined by the width of the applied load, $w$, plus a contribution from the load spreading through the depth of the member. A diagram showing these definitions is provided below in Figure 3.

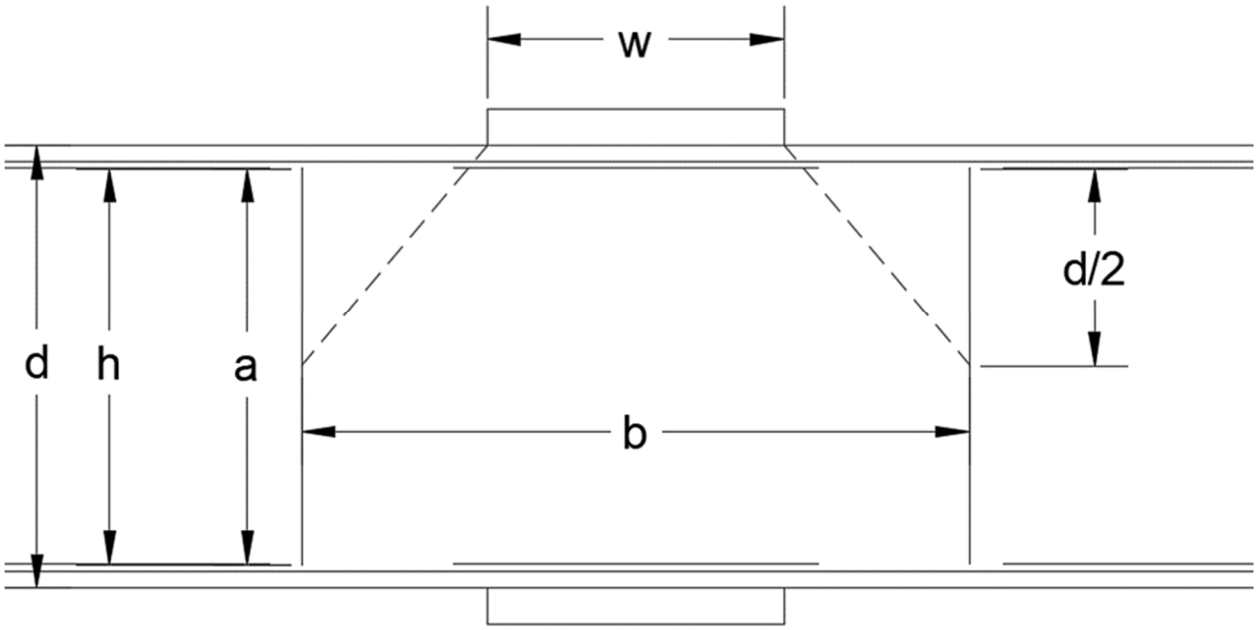


Figure 3: Diagram of Assumed Rectangular Plate

The dashed lines represent the spreading of the load from the application region to the mid-height of the web. The horizontal dimension between the intersections is the width of the assumed plate. This spread angle, $\alpha$, was determined to be 40 degrees by examining the stress contours of the finite element models at or near the peak load. Expressions for the width and depth of the buckling section of the plate geometry are provided in the following equations. The tangent of 40 degrees is approximated as 0.8 for simplicity.

$$a = h = d - 2k \tag{2}$$

$$b = w + 0.8d \tag{3}$$

*5.3 Determining Critical Elastic Buckling Load*

As mentioned previously in Chapter 5.2, the critical elastic buckling load will be used in the calculation of the final capacity of the web plate. The elastic buckling load for a rectangular, isotropic plate is given by the following equation from Timoshenko and Gere (1963):

$$P_{cr} = k * \frac{\pi^2 E t_w^3}{12(1 - v^2) * b} \tag{4}$$

$P_{cr}$ in this equation is in units of force, $E$ and $v$ are the elastic modulus (29000 ksi) and Poisson's Ratio (0.3) respectively, and the buckling factor, $k$, is a function of the aspect ratio of the plate and edge boundary conditions. Timoshenko provides an expression for $k$ when all plate edges are simply supported (SS).

$$k_{SS} = \left(\frac{1}{m}\frac{b}{a} + m\frac{a}{b}\right)^2 \tag{5}$$

However, for webs of rolled beams, it is not a valid assumption to consider the plate edges to be assumed as simply supported. The loaded edges of the plate are connected to the flanges, which provide considerable rotational restraint. Therefore, it is a more reasonable assumption to analyze these edges as fixed or clamped. The unloaded edges are neither pinned, clamped, nor free. They are continuous with the rest of the specimen, which makes classifying a boundary condition very challenging. For simplicity, the simply supported case can be modified by a constant to simulate the effect of the boundary conditions. This assumption is similar to a fixed-fixed column having an effective length of one half of a pin-ended column. Thus, the following equation for $k$ was fit for plates with loaded edges clamped, by calibrating $m$ to be equal to 0.6. The calibrated $m$ is valid for the boundary conditions of the analyzed case.

$$k = \left(1.67\frac{b}{a} + 0.6\frac{a}{b}\right)^2 \tag{6}$$

The two relationships for $k$ were compared with the eigenvalue elastic buckling strengths obtained from the numerical analysis results. Equivalent values for $k$ were obtained from the finite element results by back calculating from a known $P_{cr}$. Both the simply supported and modified equations for plate buckling are shown in Figure 4. The modification made to the original buckling equation as shown in (6) indicates the best comparison with the finite element analysis results as plotted in Figure 4. The finite element results obtained from the study conducted by Menkulasi & Farzana (2019) are consistently overpredicted because of the modeling differences between their shell elements and the solid elements used in this study.

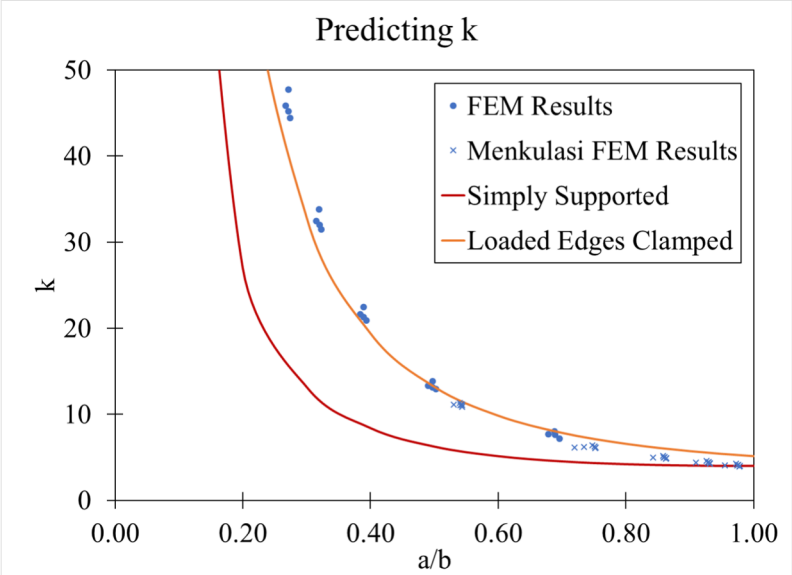

Figure 4: Plot of Numerical Results Compared with the Critical Elastic Buckling Load Equations

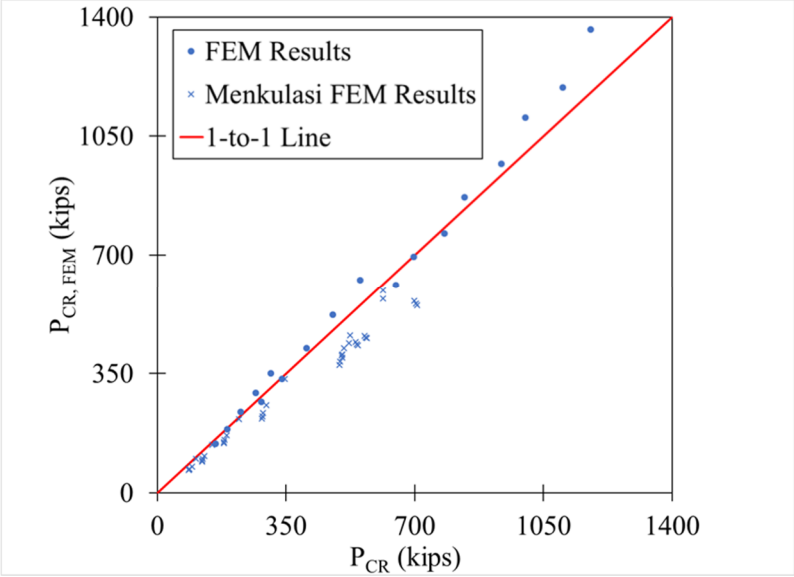

Figure 5: Comparison Plot of the Critical Elastic Load Equation

The comparison between analysis data and the prediction method can also be shown on a 1-to-1 chart. The vertical axis in Figure 5 is the analysis results and the horizontal axis is the predicted elastic buckling strength calculated from the equation for $P_{cr}$ given previously. The proposed equation estimates the analysis results well, as most of the data points lie very close to the 1-to-1 line. The proposed equation strength estimations become more conservative for specimens with larger critical buckling loads (or smaller plate slenderness ratio).

*5.4 Derivation of Buckling Strength Equation*

The buckling strength equation is derived from the principle of effective width first developed by von Kármán (1932). von Kármán showed that as the plate buckles, stresses in the plate redistribute toward the edges, as the edges are the stiffest area in the plate. He then developed an equation for

the “effective width”, which is the portion of the plate carrying most of the stress at buckling. The post-processing performed for the analysis results have indicated that a similar behavior is observed in the webs of W sections, as the stress distribution along the length of the web is displayed graphically in Figure 6.

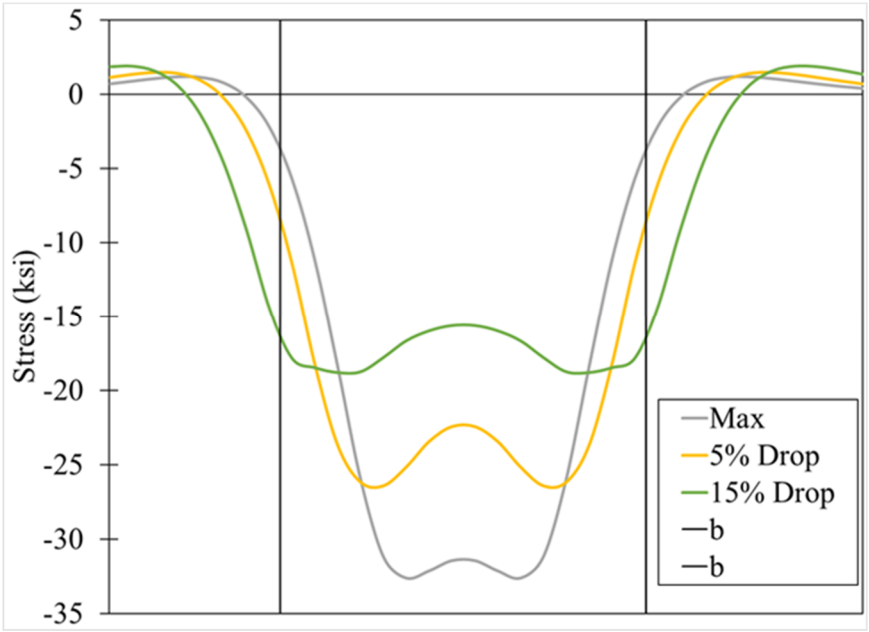

Figure 6: Plot of Average Membrane Stresses in Web at Different Load Levels

Figure 6 shows the average vertical membrane stress at the mid-height of the web variation along the member length. The vertical black lines represent the width of the effective plate, *b*. At the onset and after buckling, the average membrane stress redistributes away from the center of the effective plate as described by von Kármán. Therefore, a relationship on the basis of this effective width principle is applied for forming web compression buckling strength equations in this study.

Kalyanaraman et al. (1977) modified von Kármán’s original equation to calculate the compressive capacity of a rectangular plate as the maximum average membrane stress divided by the yield stress shown as Equation (7).

$$\frac{\sigma_{av}}{\sigma_y} = 1.19\sqrt{\frac{\sigma_c}{\sigma_y}}\left(1.0 - 0.3\sqrt{\frac{\sigma_c}{\sigma_y}}\right) = \frac{P_{ult}}{P_y} \tag{7}$$

The term $\sigma_c$ is the elastic buckling stress and $\sigma_y$ is the yield stress. The factors 1.19 and 0.3 are constants used to fit the equation to a set of experimental data from tests on thin walled, cold formed steel members. However, this equation could be used to represent web compression buckling by calibrating the constants to fit the parametric numerical results.

First, the slenderness parameter, λ, is defined as:

$$\lambda = \sqrt{\frac{\sigma_y}{\sigma_c}} = \sqrt{\frac{P_y}{P_{cr}}} \tag{8}$$

$$P_y = b * t_w * \sigma_y \tag{9}$$

Substituting the definitions from Equations (8) and (9) into Kalyanaraman's Equation (7) and representing the two constants in the equation to $A$ and $B$, yields the following equation describing the available strength in web compression buckling, $R_n$:

$$\frac{R_n}{P_y} = \frac{A}{\lambda}\left(1.0 - \frac{B}{\lambda}\right) \leq 1.0 \tag{10}$$

The upper limit of 1.0 is enforced because the buckling load cannot be greater than the plastic capacity of the web (complete yielding within the effective width). The constants $A$ and $B$ were calibrated to the mean of the numerical data by defining $A$ equal to 0.6 and $B$ equal to 0.05. The modified elastic buckling strength developed in the previous section were used for calculating $P_{cr}$ ($G_{cr}$) in the above equation. The ultimate buckling strengths obtained from the numerical FEM results are compared to this equation in Figure 7 and Figure 8.

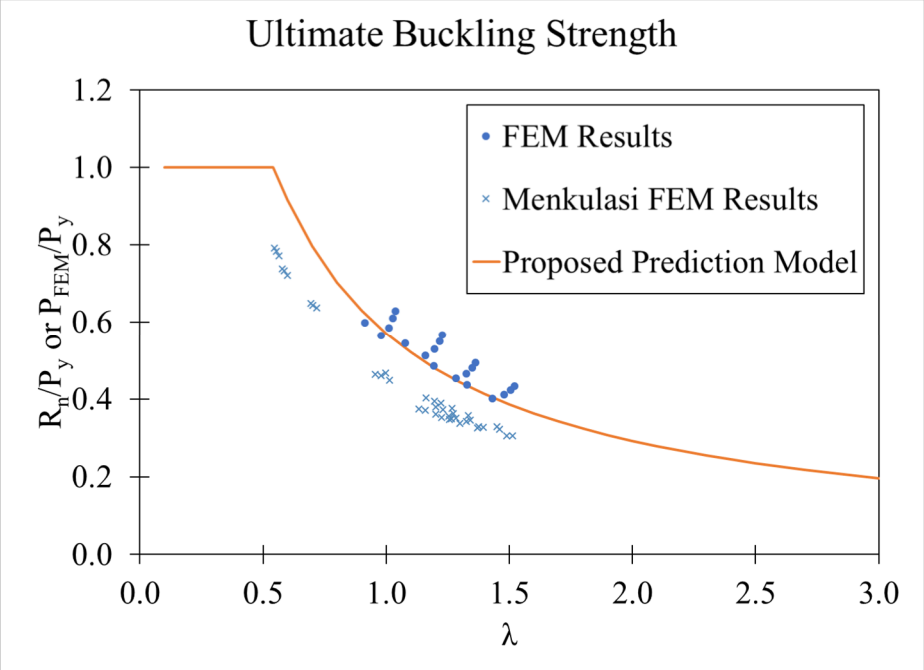


Figure 7: Ultimate Buckling Strength Plot for Vertical Load Cases

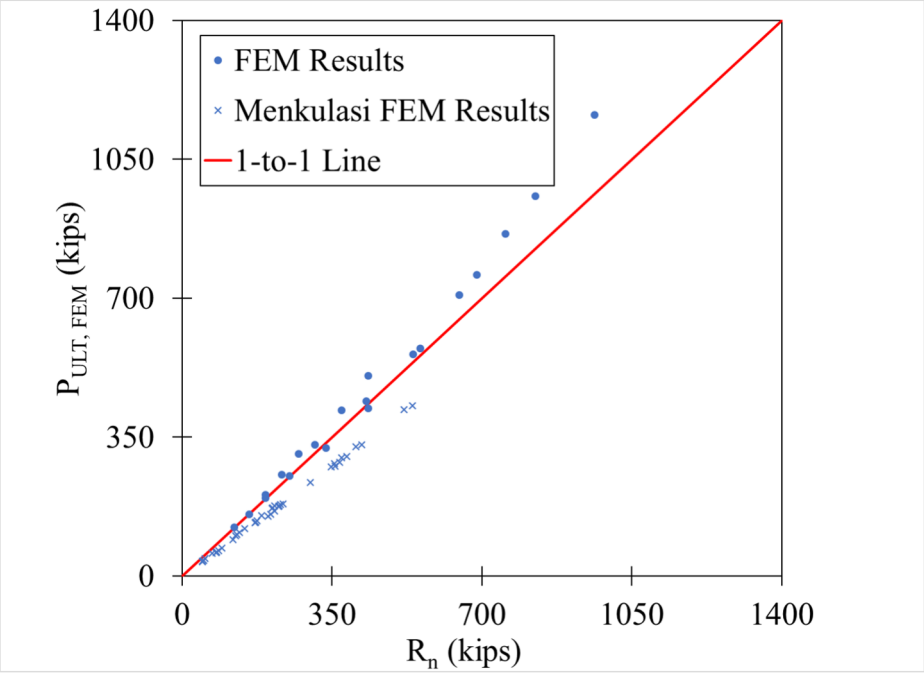

Figure 8: 1-to-1 Comparison Plot of the Ultimate Buckling Strength Equation

As shown in Figure 7, the numerical results show a strong correlation with the curve developed by Equation (10). Similar to the critical elastic strength plots, web compression buckling cases with high capacities are predicted more conservatively by the equation. The numerical analysis results obtained from Menkulasi and Farzana et al. (2016) lie below the proposed ultimate strength curve similar to the elastic buckling strength comparisons. The major discrepancy between the two data sets is attributed to the levels of imperfection assumed between the different numerical studies. The parametric study described in this paper assumed an initial imperfection magnitude of $0.13*t_w$ in accordance with physical measurements taken prior to experiments (as discussed in detail by Witte, 2019) while the other researchers assumed imperfection magnitude of *d/100* of the first mode shape, where *d* is the depth of the members. For the structural shapes included in this study, *d/100* is on average 300% larger than $0.13*t_w$, resulting in lower ultimate buckling strengths.

*5.5 Cases with Inclined Loads*

The numerical parametric study also investigated the effect of changing the angle of load application, $\theta$. This case is different from changing other parameters because the geometry of the region participating in the effective width (*b*) and the length of the web buckling length (*a*) also change. The most efficient way to tackle this problem was to treat the buckling region as an oblique plate with dimensions *a* and *b*, as shown in Figure 9.

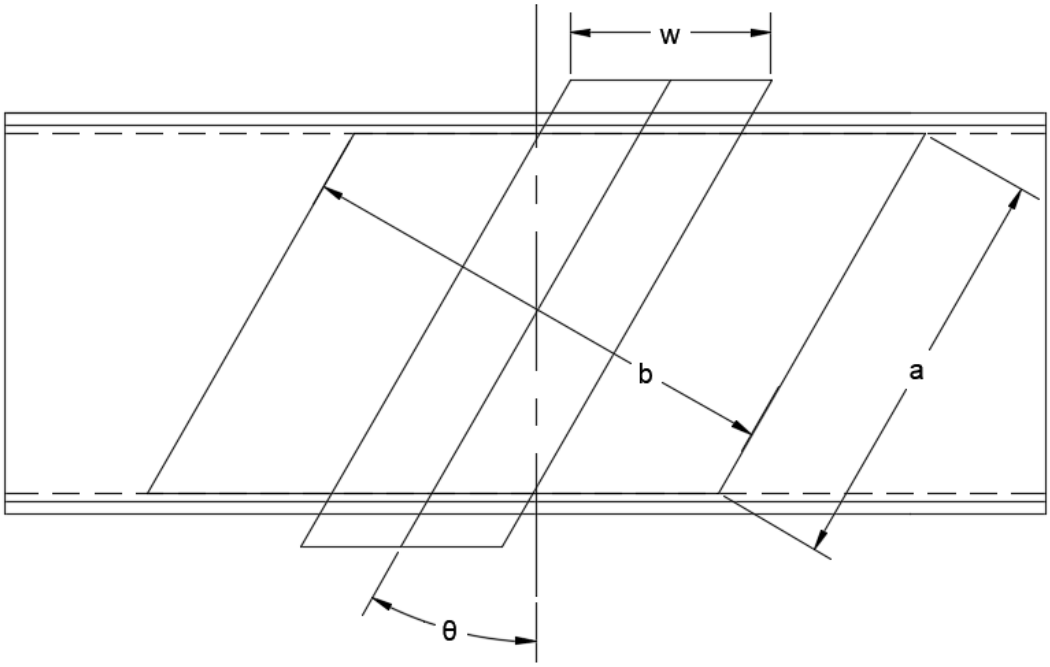

Figure 9: Oblique Web Plate Diagram

The new dimensions of $a$ and $b$ are calculated with the following equations. When $\theta$ reaches zero, these equations for the plate dimensions become the same as for the vertical cases, keeping compatibility within the models.

$$a = \frac{h}{\cos\theta} \tag{11}$$

$$b = w\cos\theta + \frac{0.8d}{\cos\theta} \tag{12}$$

As for the calculation of critical elastic buckling load, the differences between the orthogonal and oblique plates can be captured by modifying the elastic buckling coefficient, $k$. This modification is first calculated in Yoshimura et al (1963) for plate buckling and is applied to web compression buckling in this study. The modified equation for $k$ according to is given with the expression below.

$$k = \frac{k_0}{\cos^3\theta} \tag{13}$$

$$k_0 = \left(1.67\frac{b}{a} + 0.6\frac{a}{b}\right)^2 \tag{14}$$

The results from the numerical parametric study of applied loading with varying load angles are compared to the modified equations above and shown graphically in Figure 10.

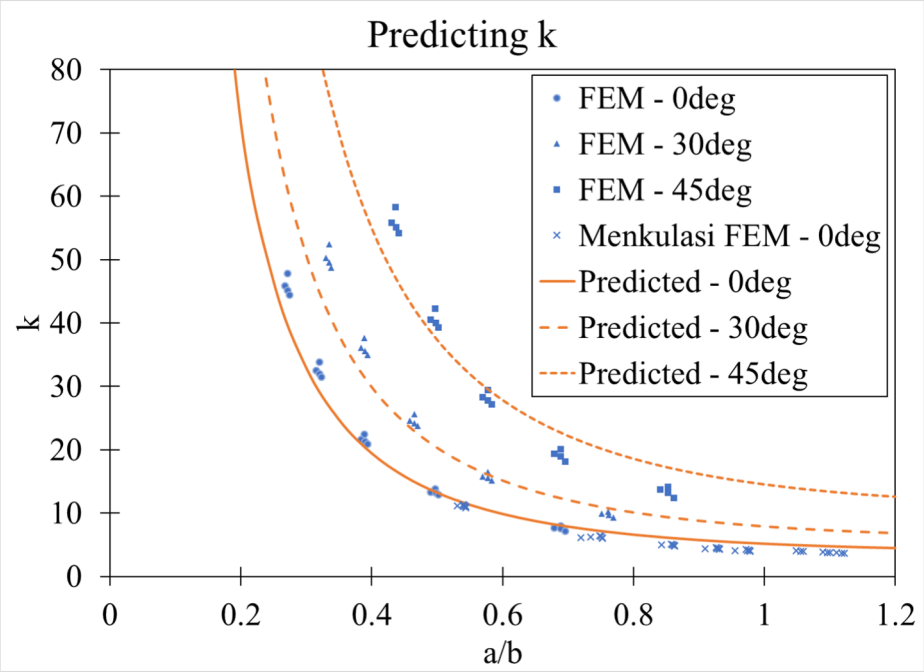

Figure 10: Plot of Numerical Results Compared with the Critical Elastic Buckling Load Equations for Inclined Load Cases

In general, Equations (13) and (14) reasonably estimate the elastic buckling strength obtained from the numerical models. The greatest discrepancy occurs for the load angle ($\theta$) of 45 degrees, as the analytical elastic buckling equation with the modified buckling coefficient overpredicts the cases with large aspect ratios and underpredict the cases with smaller aspect ratios. The reason of this discrepancy is discussed in more detail in Witte (2019).

The inclined loading effects are accounted for in the calculation of elastic buckling load, therefore the inelastic web buckling equation provided in Equation (10) is employed to calculate the strength. A plot of the numerical results from all inclined and vertical loading studies are compared with the proposed equation, as shown below in Figure 11.

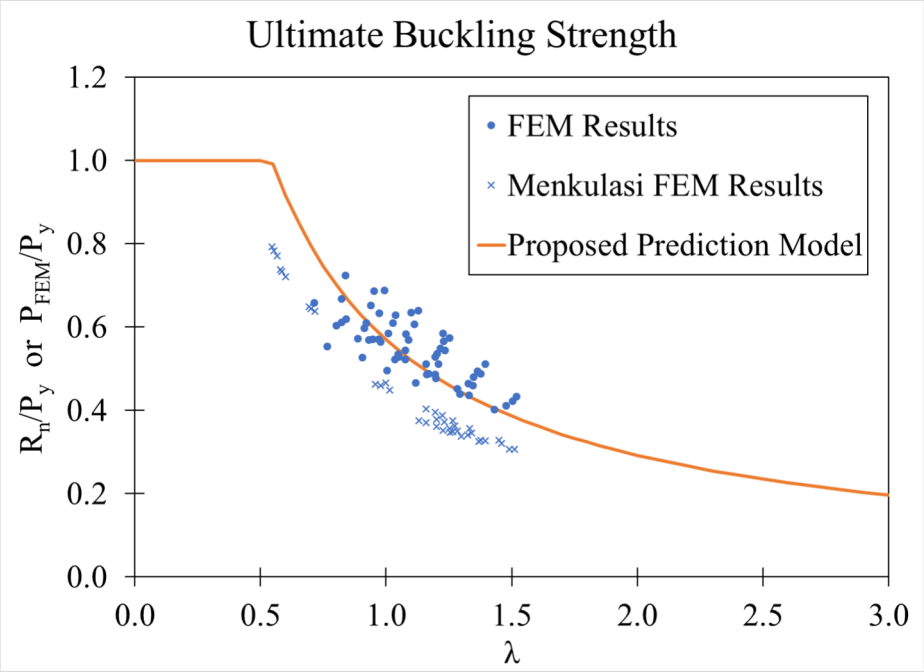

Figure 11: Ultimate Buckling Strength Plot for All Load Cases

Similar to the vertical load cases, the proposed Equation (10) reasonably predicts the strength for the numerical results for the inclined load case. The data points indicate a larger scatter with the addition of the vertical load cases of this and the other study. The reason for the large scatter is affiliated to the significant conservatism in calculating the elastic buckling coefficient for large angle cases. The analytical approach provides a consistent calculation approach by having the constants used in the elastic buckling equation remain same as the vertical cases, by *A* and *B* being equal to 0.6 and 0.05 respectively.

*5.6 Limitations of Proposed Analysis Procedure*

The proposed analysis procedure assumes isotropic material behavior through the web. Although residual stresses and strain hardening effects are not considered, it is expected that they would have negligible influence on the results obtained in this study. Residual stresses impart from differential cooling of steel members and are primarily in the longitudinal direction (in the opposite direction of web buckling). Strain hardening on the other hand initiates at very large strain levels of inelasticity and not likely to be exhibited prior to the inelastic buckling of members. All specimens analyzed in this study were assumed to have an initial web out-of-plane imperfection of 13% of the web thickness based on field measurements, as described in Witte (2019). However, this value comes from limited measurements taken from one size of beam and may not be representative and applicable to all the steel shapes investigated in the parametric study. Some discrepancy may occur due to this assumption and the coefficients *A* and *B* used in Equation (10) may be altered for different imperfection levels.

The analysis procedure was developed by considering member depths varying between 16 and 24 inches. Structural steel members that lie outside of these depths may exhibit slightly different behavior. The numerical results were limited to load widths up to 2.5 times the section depth of structural shape. For larger width to depth ratios, the procedure is expected to remain accurate, but

with greater uncertainty. The specimens were also analyzed under uniformly distributed load case; therefore, the analysis procedure is valid for only this case. As shown in Figure 10, the accuracy of the procedure diminishes for large values of $\theta$, so it is advised to incorporate more detailed supplemental analysis for such cases.

## 6. Conclusions

This paper builds upon the authors' previous experimental research to provide an analytical analysis method for calculating the web compression buckling strength of wide flanged steel members more accurately than the current guidance provided in the AISC 360 specification. In lieu of providing a method to incorporate load width into Equation J10-8, the commentary of AISC 360 suggests analyzing those cases as compression members (columns) according to the provisions of Chapter E. This method was found to be an adequate, but overly conservative estimation for estimating the strength of the web compression buckling limit state. The method proposed in this paper analyzes the web as a rectangular plate subject to uniform compression. The dimensions of the plate are based on the effective width of web participating in force resistance determined from the numerical modeling results. Using the assumed plate dimensions and boundary conditions, the elastic buckling and ultimate buckling loads are calculated. This proposed analytical calculation method has been demonstrated to predict web compression buckling strength more accurately than the current design provisions in the AISC specification.

## Acknowledgments

This research was funded by Veolia Water Technologies and conducted at Purdue University's Bowen Laboratory for Large Scale Engineering Research. The steel specimens were donated by Steel Dynamics, Inc. The authors would also like to thank Research Engineer Tom Bradt for his assistance and direction in conducting the experiments and Dr. Cem Korkmaz for his assistance in conducting the numerical parametric study.

## References

AISC Committee. (2010). Specification for structural steel buildings (ANSI/AISC 360-10). *American Institute of Steel Construction, Chicago-Illinois*.

Kalyanaraman, V., Winter, G., & Pekoz, T. (1977). Unstiffened compression elements. *Journal of the Structural Division*, *103*(9), 1833-1848.

Menkulasi, F., & Farzana, N. (2019). Web compression buckling capacity prediction for unstiffened I-sections with opposite patch loading.*Journal of Constructional Steel Research*,*162*, 105728.

Menkulasi, F., Farzana, N., Moen, C.D., Eatherton, M.R. (2016). "Revisiting Web Compressing Buckling for Wide Flange Sections" *Proceedings of the Annual Stability Conference.* Orlando, FL. April 12-15, 2016.

Sener, K., Witte, J., Varma, A.H. (2019). "On the influence of load width on web compression buckling strength" *Proceedings of the Annual Stability Conference.* St. Louis, MO. April 2-5, 2019.

Timoshenko, S. P., & Gere, J. M. (1963). *Theory of elastic stability*. McGraw-Hill Book Company, Inc.

von Kármán, T., Sechler, E. E., and Donnell, L. H. (1932). Strength of Thin Plates in Compression. *Trans. ASME*, *54*, 53-57.

Witte, Jacob. (2019). *Influence of loading width on web compression buckling of steel beams*. Master's Thesis. Purdue University, West Lafayette, Indiana.

Yoshimura, Y., & Iwata, K. (1963). Buckling of simply supported oblique plates. *Journal of Applied Mechanics*, *30*(3), 363-366.

Ziemian, R. D. (Ed.). (2010). *Guide to stability design criteria for metal structures*. John Wiley & Sons.